Synthesis of Water-Soluble and Functionalized Nanoparticles by Silica Coating

Nikhil R. Jana, Christopher Earhart, and Jackie Y. Ying*

Institute of Bioengineering and Nanotechnology, 31 Biopolis Way, The Nanos, Singapore 138669

Received May 21, 2007

Synthetic methods for high-quality near-monodispersed nanoparticles of metals, metal oxides, and quantum dots in organic solvents are well-developed, but their applications are restricted due to the lack of water solubility and tailored surface chemistry. In this work, we report the silica-coating procedure for various hydrophobic nanoparticles, including Au, Ag, Fe_3O_4, and ZnS−CdSe to derive water-soluble and functionalized nanoparticles. We have developed a silica-coating method in toluene using commercially available silanes. This approach is applicable to hydrophobic nanoparticles in the size range of 2−20 nm. Silica-coated nanoparticles are 10−30 nm in size, water-soluble, buffer-stable, and have a positive or negative surface charge depending on the surface functional group and solution pH. The coated particles have primary amine groups on the outer surface and are further functionalized with biotin and antibody.

Introduction

Nanoparticles of a 1−100 nm size have broad applications in biology such as biolabeling, imaging, drug delivery, separation, and optical sensing.[1] The size of nanoparticles plays an important role in determining their properties,[1] as well as their usefulness in bioapplications.[2] Additionally, nanoparticles need to be water-soluble and colloidally stable with a tailored surface chemistry. Most syntheses for high-quality, near-monodispersed nanoparticles of semiconductors,[3] metals,[4] and metal oxides[5] involved nonaqueous solvents and coating with monolayers of hydrophobic surfactants. Such nanoparticles could not be used directly for biofunctionalization as they were water-insoluble and did not have suitable functional groups for bioconjugation. Several strategies have been developed to tackle these challenges, such as exchanging the original stabilizer with thiols,[6] dendrons,[7] oligomeric phosphine,[8] polymer coating[9] and silica coating.[10−15] The key was to control the sensitive surface chemistry of the nanoparticles and the colloidal stability of the nanoparticles in aqueous phase. It has been observed that ligand-exchanged nanoparticles were not stable in adverse conditions since the weakly adsorbed organic shell would desorb from the nanoparticle surface.[6b] Thus, a cross-

* Corresponding author. E-mail: jyying@ibn.a-star.edu.sg.

(1) (a) Eugenii, K.; Willner, I. *Angew. Chem., Int. Ed.* **2004**, *43*, 6042. (b) Michalet, X.; Pinaud, F. F.; Bentolila, L. A.; Tsay, J. M.; Doose, S.; Li, J. J.; Sundaresan, G.; Wu, A. M.; Gambhir, S. S.; Weiss, S. *Science* **2005**, *307*, 538. (c) Nam, J. M.; Thaxton, C. S.; Mirkin, C. A. *Science* **2003**, *301*, 1884. (d) Tiefenauer, L. X.; Kuehne, G.; Andres, R. Y. *Bioconjugate Chem.* **1993**, *4*, 347. (e) Kim, S.; Lim, Y. T.; Soltesz, E. G.; De Grand, A. M.; Lee, J.; Nakayama, A.; Parker, J. A.; Mihaljevic, T.; Laurence, R. G.; Dor, D. M.; Cohn, L. H.; Bawendi, M. G.; Frangioni, J. V. *Nat. Biotechnol.* **2004**, *22*, 93.

(2) (a) Mahtab, R.; Rogers, J. P.; Murphy, C. J. *J. Am. Chem. Soc.* **1995**, *117*, 9099. (b) Chen, F.; Gerion, D. *Nano Lett.* **2004**, *4*, 1827. (c) Osaki, F.; Kanamori, T.; Sando, S.; Sera, T.; Aoyama, Y. *J. Am. Chem. Soc.* **2004**, *126*, 6520.

(3) (a) Murray, C. B.; Norris, D. J.; Bawendi, M. G. *J. Am. Chem. Soc.* **1993**, *115*, 8706. (b) Li, J. J.; Wang, Y. A.; Guo, W.; Keay, J. C.; Mishima, T. D.; Johnson, M. B.; Peng, X. *J. Am. Chem. Soc.* **2003**, *125*, 12567.

(4) (a) Brust, M.; Walker, M.; Bethell, D.; Schiffrin, D. J. *J. Chem. Soc., Chem. Commun.* **1994**, 801. (b) Sun, S.; Murray, C. B.; Weller, D.; Folks, L.; Moser, A. *Science* **2000**, *287*, 1989. (c) Jana, N. R.; Peng, X. *J. Am. Chem. Soc.* **2003**, *125*, 14280.

(5) (a) Hyeon, T.; Lee, S. S.; Park, J.; Chung, Y.; Na, H. B. *J. Am. Chem. Soc.* **2001**, *123*, 12798. (b) Sun, S.; Zeng, H. *J. Am. Chem. Soc.* **2002**, *124*, 8204. (c) Jana, N. R.; Chen, Y.; Peng, X. *Chem. Mater.* **2004**, *16*, 3931.

(6) (a) Templeton, A. C.; Wuelfing, W. P.; Murray, R. W. *Acc. Chem. Res.* **2000**, *33*, 27. (b) Aldana, J.; Lavelle, N.; Wang, Y.; Peng, X. *J. Am. Chem. Soc.* **2005**, *127*, 2496.

(7) (a) Guo, W.; Li, J. J.; Wang, Y. A.; Peng, X. *J. Am. Chem. Soc.* **2003**, *125*, 3901. (b) Guo, W.; Li, J. J.; Wang, Y. A.; Peng, X. *Chem. Mater.* **2003**, *15*, 3125. (c) Kim, M.; Chen, Y.; Liu, Y.; Peng, X. *Adv. Mater.* **2005**, *17*, 1429.

(8) Kim, S.-w.; Kim, S.; Tracy, J. B.; Jasanoff, A.; Bawendi, M. G. *J. Am. Chem. Soc.* **2005**, *127*, 4556.

(9) (a) Gao, X.; Cui, Y.; Levenson, R. M.; Chung, L. W. K.; Nie, S. *Nat. Biotechnol.* **2004**, *22*, 969. (b) Pellegrino, T.; Manna, L.; Kudera, S.; Liedl, T.; Koktysh, D.; Rogach, A. L.; Keller, S.; Radler, J.; Natile, G.; Parak, W. J. *Nano Lett.* **2004**, *4*, 703.

(10) (a) Liz-Marzán, L. M.; Giersig, M.; Mulvaney, P. *Langmuir* **1996**, *12*, 4329. (b) Buining, P. A.; Humbel, B. M.; Philipse, A. P.; Verkleij, A. J. *Langmuir* **1997**, *13*, 3921. (c) Bharathi, S.; Fishelson, N.; Lev, O. *Langmuir* **1999**, *15*, 1929. (d) Obare, S. O.; Jana, N. R.; Murphy, C. J. *Nano Lett.* **2001**, *1*, 601. (e) Schroedter, A.; Weller, W. *Angew. Chem., Int. Ed.* **2002**, *41*, 3218. (f) Kobayashi, Y.; Horie, M.; Konno, M.; Rodriguez-Gonzalez, B.; Liz-Marzán, L. M. *J. Phys. Chem. B* **2003**, *107*, 7420. (g) Graf, C.; Vossen, D. L. J.; Imhof, A.; van Blaaderen, A. *Langmuir* **2003**, *19*, 6693. (h) Kobayashi, Y.; Katakami, H.; Mine, E.; Nagao, D.; Konno, M.; Liz-Marzán, L. M. *J. Colloid Interface Sci.* **2005**, *283*, 392.

(11) (a) Fan, H. Y.; Chen, Z.; Brinker, C. J.; Clawson, J.; Alam, T. *J. Am. Chem. Soc.* **2005**, *127*, 13746. (b) Lee, D. C.; Mikulec, F. V.; Pelaez, J. M.; Koo, B.; Korgel, B. A. *J. Phys. Chem. B* **2006**, *110*, 11160.

(12) (a) Liu, X.; Xing, J.; Guan, Y.; Shan, G.; Liu, H. *Colloids Surf., A* **2004**, *238*, 127. (b) Veiseh, O.; Sun, C.; Gunn, J.; Kohler, N.; Gabikian, P.; Lee, D.; Bhattarai, N.; Ellenbogen, R.; Sze, R.; Hallahan, A.; Olson, J.; Zhang, M. *Nano Lett.* **2005**, *5*, 1003.

(13) (a) Woo, K.; Hong, J.; Ahn, J.-P. *J. Magn. Magn. Mater.* **2005**, *293*, 177. (b) Yi, D. K.; Selvan, S. T.; Lee, S. S.; Papaefthymiou, G. C.; Kundaliya, D.; Ying, J. Y. *J. Am. Chem. Soc.* **2005**, *127*, 4990. (c) Yi, D. K.; Lee, S. S.; Papaefthymiou, G. C.; Ying, J. Y. *Chem. Mater.* **2006**, *18*, 614. (d) Kim, J.; Lee, J. E.; Lee, J.; Yu, J. H.; Kim, B. C.; An, K.; Hwang, Y.; Shin, C.-H.; Park, J.-G.; Kim, J.; Hyeon, T. *J. Am. Chem. Soc.* **2006**, *128*, 688. (e) Jana, N. R.; Yu, H.-h.; Mohamed Ali, E.; Zheng, Y.; Ying, J. Y. *Chem. Commun.* **2007**, 1406.

10.1021/cm071368z CCC: $37.00
Published on Web 09/18/2007

coupling between ligands has often been used after ligand exchange so as to provide a covalent bridge surrounding the particles.[9]

Silica coating is one of the most popular techniques for nanoparticle surface modification.[10−15] This coating method can introduce a cross-linked silica shell to protect the core nanoparticles from the external environment. It can be used for hydrophilic[10,12,14] and hydrophobic[11,13,15] nanoparticles of metals,[10,11] metal oxides,[12,13] and quantum dots (QDs)[14,15] in a size range of 1−100 nm. Although numerous methods have been published on silica coating, only a few methods have reported silica-coated nanoparticles <20 nm in size with a high water solubility and colloidal stability.[10e,14b,15a,b,i] The typical silica-coated particles are >25 nm in size and can be as large as several micrometers. Finer particles are important in biomedical applications to reduce nonspecific interactions, minimize steric effects, and provide a higher clearance rate.[16]

Polymerization of silane monomers in the presence of nanoparticles under Stöber's condition[17] is widely used as it provides uniform silica coating with a controllable thickness and produces particles of 50 nm to several micrometers. Stöber's condition involves alcohol−water−ammonia as the media and tetraethoxysilane (TEOS) as the silane monomer. However, the formation of insoluble silica−nanoparticle aggregates is a common problem due to the sensitive surface chemistry of nanoparticles. Preparation of finer core−shell particles by this method is also difficult as particles with thin silica coatings have a very high tendency to aggregate, leading to multicore formation within the silica shell. In the case of hydrophobic nanoparticles, Stöber's condition is difficult to apply as the nanoparticles are insoluble in the alcohol−water media. Various modifications have been reported for the effective silica coating of hydrophobic nanoparticles. These included the modification of Stöber's condition (e.g., reverse micelle or microemulsion,[11b,13b,15d,f,j] polymer[10g]/surfactant[10d] stabilizer), the use of lipophilic silane monomers,[11a,15i] the use of trialkoxysilanes[10e,14b,15a] that minimized the shell thickness, and the application of hydrophilic silanes[15a,b] that induced water solubility for the final nanoparticles.

Previously, we reported a reverse micelle based approach for silica coating of hydrophobic QDs and iron oxide.[13b,c,15h,l] Using this approach, a thick silica coating was achieved using TEOS as the silane monomer. Although the shell was uniform and the shell thickness could be varied from 2 to 50 nm (with an overall particle size of >25 nm), the thin silica shell-coated particles have a lower colloidal stability, higher aggregation tendency, and tended to form asymmetric shells with multiple cores.[13c] We presumed that the dynamic nature of the reverse micelles, the presence of excess surfactants, and the use of the TEOS reagent induced such problems. Recently, we reported the silica coating of hydrophobic ZnO in toluene using trimethoxysilanes as reagents.[13e] The current study extended the silica coating in the toluene phase to hydrophobic Au, Ag, Fe_3O_4, and QDs. There were three significant modifications as compared to our earlier reverse micelle based approach. First, toluene was used as the coating medium instead of reverse micelles. Second, TEOS was replaced by trimethoxysilane or trihydroxysilane that terminated silica polymerization and restricted the thick silica shell formation. Third, silica polymerization was controlled by the temperature and base catalyst. The current method could be used for a wide variety of hydrophobic nanoparticles synthesized by nonaqueous routes. Hydrophobic nanoparticles were reacted with silane in toluene to obtain a nanoparticle−silane conjugate. Both the hydrophobic nanoparticles and the silanes could be solubilized in toluene, but the silanized particles would be precipitated from this phase. Precipitation of silanized nanoparticles limited the silica-coating thickness on the particle surface, inhibited the particle−particle cross-linking, and produced water-soluble coated nanoparticles of finer sizes. In earlier approaches, a thin silica coating on QDs was developed in hydrophilic solvents via a multistep process, which included the ligand exchange of hydrophobic nanoparticles, silane hydrolysis in alcohol, and quenching of excess silanes.[15a] In another approach, Au nanoparticle synthesis and silica coating were carried out in alcohol, but this method could not produce near-monodispersed nanoparticles of tailored sizes.[10b,e] In this current method, the hydrophobic particles were first synthesized in an organic phase via the established routes and then coated with silica in toluene. This method presented the following advantages: (i) it was simple, highly reproducible, and could be easily scaled up from milligrams to multigrams; (ii) it could be applied to a variety of hydrophobic nanoparticles, such as Au, Ag, Fe_3O_4, and QDs; (iii) various commercially available silanes could be used in the silica coating; (iv) thin silica shells of 2−5 nm in thickness could be attained; and (v) the silanized particles were near-monodispersed and have a high water solubility and colloidal stability.

Experimental Procedures

Materials. Didodecyldimethylammonum bromide (DDAB) (TCI), dodecylamine (Sigma), decanoic acid (DA) (Sigma), tetrabutylammonium borohydride (TBAB) (Sigma), tetramethyl ammonium hydroxide pentahydrate (TMAH) (Sigma), anhydrous $AuCl_3$ (Sigma),

(14) (a) Correa-Duarte, M. A.; Giersig, M.; Liz-Marzán, L. M. *Chem. Phys. Lett.* **1998**, *286*, 497. (b) Schroedter, A.; Weller, H.; Eritja, R.; Ford, W. E.; Wessels, J. M. *Nano Lett.* **2002**, *2*, 1363. (c) Wolcott, A.; Gerion, D.; Visconte, M.; Sun, J.; Schwartzberg, A.; Chen, S.; Zhang, J. Z. *J. Phys. Chem. B* **2006**, *110*, 5779.

(15) (a) Bruchez, M.; Moronne, M.; Gin, P.; Weiss, S.; Alivisatos, A. P. *Science* **1998**, *281*, 2013. (b) Gerion, D.; Pinaud, F.; Williams, S. C.; Parak, W. J.; Zanchet, D.; Weiss, S.; Alivisatos, A. P. *J. Phys. Chem. B* **2001**, *105*, 8861. (c) Parak, W. J.; Gerion, D.; Zanchet, D.; Woerz, A. S.; Pellegrino, T.; Micheel, C.; Williams, S. C.; Seitz, M.; Bruehl, R. E.; Bryant, Z.; Bustamante, C.; Bertozzi, C. R.; Alivisatos, A. P. *Chem. Mater.* **2002**, *14*, 2113. (d) Kohler, N.; Fryxell, G. E.; Zhang, M. *J. Am. Chem. Soc.* **2004**, *126*, 7206. (e) Nann, T.; Mulvaney, P. *Angew. Chem., Int. Ed.* **2004**, *43*, 5393. (f) Chan, Y.; Zimmer, J. P.; Stroh, M.; Steckel, J. S.; Jain, R. K.; Bawendi, M. G. *Adv. Mater.* **2004**, *16*, 2092. (g) Liedl, T.; Keller, S.; Simmel, F. C.; Radler, J. O.; Parak, W. J. *Small* **2005**, *1*, 997. (h) Selvan, S. T.; Tan, T. T.; Ying, J. Y. *Adv. Mater.* **2005**, *17*, 1620. (i) Darbandi, M.; Thomann, R.; Nann, T. *Chem. Mater.* **2005**, *17*, 5720. (j) Darbandi, M.; Lu, W.; Fang, J.; Nann, T. *Langmuir* **2006**, *22*, 4371. (k) Zhelev, Z.; Ohba, H.; Bakalova, R. *J. Am. Chem. Soc.* **2006**, *128*, 6324. (l) Selvan, S. T.; Patra, P. K.; Ang, C. Y.; Ying, J. Y. *Angew. Chem., Int. Ed.* **2007**, *46*, 2448. (m) Tan, T. T.; Selvan, S. T.; Zhao, L.; Gao, S.; Ying, J. Y. *Chem. Mater.* **2007**, *19*, 3112.

(16) Allemann, E.; Gurny, R.; Doelker, E. *Eur. J. Pharm. Biopharm.* **1993**, *39*, 173.

(17) Stöber, W.; Fink, A.; Bohn, E. *J. Colloid Interface Sci.* **1968**, *26*, 62.

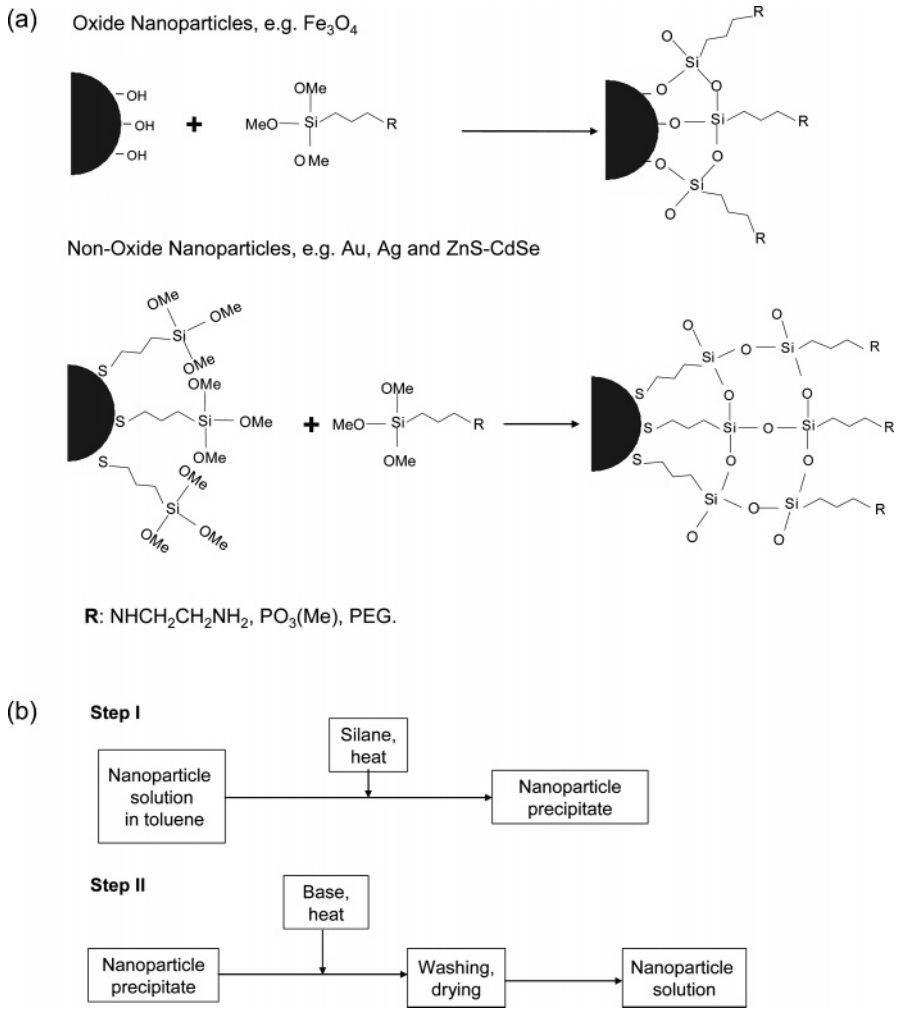

Figure 1. (a) Silane conjugation chemistry for different types of nanoparticles. (b) Scheme for two-step silanization of nanoparticles.

silver acetate (Sigma), Tween 80 (Sigma), and bis[2-(*N*-succinimidyl-succinylamino)-ethyl]polyethylene glycol-3000 (NHS-PEG-NHS) (Fluka) were used as received. IgG from human serum (h-IgG), anti-human goat-raised IgG (goat anti-h-IgG), and bovine serum albumin (BSA) were purchased from Sigma. 3-Mercaptopropyltrimethoxysilane (MPS) (Lancaster), 2-aminoethyl-aminopropyltrimethoxysilane (AEAPS) (Merck), 2-methoxy(polyethyleneoxy)propyltrimethoxysilane (PEG silane) (Gelest), 3-trihydroxysilylpropyl methyl phosphonate sodium salt (42% in water) (phosphonate silane) (ABCR), and (*N*,*N*-dimethylaminopropyl)-trimethoxysilane (Aldrich) were used as received, without further purification.

All silane solutions (0.1 M) were prepared in toluene except for phosphonate silane, which was prepared in methanol. Fresh stock solutions were prepared daily since silanes are reactive to moisture.

Synthesis of Nanoparticles. Near-monodispersed Au and Ag nanoparticles of a 2−10 nm size were prepared in toluene according to our previous report.[4c] Near-monodispersed Fe_3O_4 nanoparticles of a 4−15 nm size were prepared by the high-temperature pyrolysis of Fe(II) carboxylate salt in octadecene.[5c] CdSe was prepared with carboxylate precursors in octadecene by the high-temperature synthesis route.[3b] CdSe nanoparticles were purified from free ligands and capped by a ZnS shell at 200 °C in octadecene via the alternate injection of Zn stearate in octadecene and elemental S dissolved in octadecene.[3b]

General Procedure for Silane Conjugation. The silanization scheme is shown in Figure 1a. Silanization of Fe_3O_4 nanoparticles involved the direct condensation of their surface hydroxide species with silyl groups. In the case of Au, Ag, and ZnS−CdSe QDs, a linker silane (MPS) was used in addition to other silanes. Two-step silanization was used for better coating in the case of Fe_3O_4 and other oxide nanoparticles, whereas only the first step was used for coating Au, Ag, and QDs (Figure 1b). The general procedure for silane conjugation is described next, and the method can be applied to other silanes.

Silica Coating of Fe_3O_4 Nanoparticles. As-synthesized Fe_3O_4 nanoparticles were purified and separated from free ligands by a standard precipitation−redispersion scheme. In a typical purification process, 0.5 mL of a nanoparticle solution (0.2 M in terms of iron) was mixed with 0.5 mL of toluene and then precipitated with 1 mL of acetone. The mixture was centrifuged at 14 000 rpm for 2 min, and the supernatant was discarded. The precipitate was then dissolved in 1 mL of toluene and further precipitated by adding 1 mL of ethanol. The mixture was then heated at 50 °C for 1 min and centrifuged at 25 000 rpm for 2 min. The precipitate was redispersed in toluene and precipitated again by ethanol, followed by centrifugation. This precipitation−redispersion procedure was repeated 2 more times, and the particles obtained were dissolved in 2 mL of toluene prior to silica coating.

In a typical silica-coating process, the purified toluene solution (2 mL) was mixed with 1.0 mL of toluene solution with 0.01 M AEAPS (or other silane or mixed silanes), followed by the addition of 1 mL of a methanol solution of TMAH (0.01 M). The mixture was stirred by a magnetic stirrer and heated to 80 °C for 10 min until complete precipitation. Next, the supernatant was discarded, and the particles were washed with toluene. In the second step, the

solid precipitate was mixed with 3 mL of toluene and 1 mL of ethanol solution of TMAH (0.01 M) and heated to 80 °C for 15 min. The solid precipitate obtained was washed repeatedly in toluene and/or ethanol and then dissolved in 1 mL of water. In the case of insoluble precipitate, 10−100 μL of an aqueous formic acid solution (0.1 M) was added to solubilize the particles.

Phosphonate silane was introduced under a slightly different condition as this silane is not soluble in toluene. It was solubilized in methanol, and silanization was carried out in a toluene−methanol mixture with a 50−75 vol % of toluene. A total of 0.5 mL of iron oxide solution was diluted to 2 mL with toluene and then mixed with 1 mL of methanol solution of phosphonate silane (0.01 M) and 1 mL of methanol solution of TMAH (0.01 M). When mixed silanes were used, the nanoparticle solution was mixed with different volumes of AEAPS and phosphonate silane, while keeping the total volume to 1 mL. Next, 1 mL of TMAH (0.01 M) solution in ethanol was added. Other steps of the synthesis procedure remained unchanged. The washed precipitate was dissolved in phosphate buffer (pH 9.5).

Silica Coating of Au Nanoparticles. A total of 10 mL of $AuCl_3$ solution (0.01 M) was prepared in toluene in the presence of an equimolar amount of DDAB. Next, 200 μL of a toluene solution of MPS (0.1 M) was added. A total of 1 mL of toluene solution of TBAB (produced by sonicating 25 mg of TBAB and 25 mg of DDAB in toluene) was then added under stirring to reduce the gold salt, producing 2−3 nm sized gold nanoparticles in a pink solution. Next, 2 mL of toluene solution of AEAPS (0.1 M) (or a mixture of 2 mL of AEAPS and 0.5 mL of PEG silane) was added, and the resulting solution was heated to 65 °C. Particles began precipitating after 3−4 min and were completely precipitated after 15 min. The precipitate was washed twice with toluene, twice with chloroform, and twice with 100% ethanol. Next, it was solubilized in 2 mL of deionized water, forming a dark brown solution that was stable for several months. The core size of the gold particles would grow to 4−5 nm (as confirmed by TEM) during the heating step, and the overall core−shell particle size was 6−10 nm (as determined by dynamic light scattering (DLS)).

To prepare larger gold nanoparticles, the particles were synthesized first and then subjected to silica coating. Typically, 5−6 nm sized gold nanoparticles were prepared by injecting a toluene solution of TBAB (produced by sonicating 25 mg of TBAB and 25 mg of DDAB in toluene) into 10 mL of toluene solution of $AuCl_3$ (0.01 M), which was prepared in the presence of 0.01 M DDAB and 0.1 M DA. Next, 50 μL of MPS solution and 500 μL of AEAPS were added, followed by heating for 30 min. The precipitate was washed as before and then dissolved in water. These particles have a lower solubility in water, but the solubility could be increased by lowering the solution pH with acidic buffer solution or formic acid solution. The gold core size was 6−7 nm (as confirmed by TEM), and the overall core−shell particle size was 10−15 nm (as determined by DLS).

Silica Coating of Ag Nanoparticles. A total of 17 mg of CH_3-COOAg was dissolved by sonication in 10 mL of toluene in the presence of 72 mg of dodecylamine. An optically clear solution was formed. Next, 200 μL of toluene solution of MPS (0.1 M) was added. A total of 1 mL of toluene solution of TBAB (produced by sonicating 25 mg of TBAB and 17 mg of DA in toluene) was added under stirring. (***Caution!*** *Be careful of hydrogen gas formation during mixing.*) A yellow solution of silver nanoparticles was produced. Next, 2 mL of the toluene solution of AEAPS (0.1 M) was added, and the entire solution was heated to 65 °C for 15−30 min or until complete precipitation. The solution was centrifuged at 14 000 rpm for 3−4 min, and the supernatant was removed. The precipitate was washed repeatedly with toluene, chloroform, and ethanol and then solubilized in 2 mL of deionized water to form a brown solution. The core size of the Ag particles was 3−5 nm (as confirmed by TEM), and the overall core−shell particle size was 9−12 nm (as determined by DLS).

To prepare larger silver particles, the synthesis was first conducted in the absence of MPS. Then, MPS (50 μL) and AEAPS (500 μL) were added for silica coating. All other conditions remained unchanged. The core size of the Ag particles was 6−8 nm (as confirmed by TEM), and the overall core−shell particle size was 10−20 nm (as determined by DLS).

Silica Coating of QDs. As-synthesized ZnS−CdSe QDs were purified by the standard precipitation−redispersion procedure as described for Fe_3O_4, and a toluene solution of QDs was prepared (absorbance = 0.5−1.0 at the first absorption peak). Next, 0.5 mL of the stock solution was diluted with 3.5 mL of toluene and mixed with 4 μL of MPS, 20 μL of AEAPS, and 20 μL of PEG silane. The resulting solution was heated to 65 °C under stirring. The particles began precipitating within 3−4 min, and heating was continued for 10 min. The precipitate was washed with toluene, chloroform, and ethanol. It was then dissolved in 4-morpholineethanesulfonic acid (MES)/*N*-(2-hydroxyethyl)piperazine-*N*′-(2-ethanesulfonic acid) sodium salt (HEPES) buffer (pH 6.0). This method produced completely water-soluble particles. The overall core−shell particle size was 9−15 nm (as determined by DLS).

Bioconjugation and Immunoassay Protocol. When AEAPS was used as silane monomer, the silica coating presented surface primary amine groups. The resulting primary amine-functionalized particles were used for bioconjugation experiments. The primary amine groups on the particle surface were covalently linked with the primary amine groups of the antibodies using a conventional bifunctional PEG reagent (NHS-PEG-NHS). The conjugation procedure was similar to the protein conjugation protocol with the primary amine-functionalized nanoparticles provided by Invitrogen. One NHS group would react with the primary amine group of the particle, and the other NHS group would react with the antibody. A NHS-biotin reagent was used to prepare the biotinylated particles; the NHS group would react with the primary amine group of the particle. The conjugation procedure is described as follows: 0.05 mL of the silanized gold particle solution was diluted with 1 mL of borate buffer (pH 7.5) and mixed with a *N*-hydroxysuccinimide (NHS)-PEG-biotin solution (1 mg/mL dimethylformamide (DMF)) or a bifunctional NHS-PEG-NHS solution (produced by dissolving 10 mg of NHS-PEG-NHS in 100 μL of dry dimethylsulfoxide (DMSO)). Biotinylated particles were dialyzed after 2 h of incubation and preserved at 4 °C. NHS-PEG-NHS-conjugated particles were passed through a Sephadex G25 column after a short incubation (15 min) to separate the free reagents from the Au particles. The solution of activated particles was immediately mixed with 200 μL of goat anti-h-IgG solution (2 mg/mL) and kept at 4 °C for 1 h. It was then purified free of antibodies and excess reagents by centrifuging at 25 000 rpm for 30 min. The precipitate was dissolved in 1.0 mL of Tris buffer (pH 7.0) and preserved at 4 °C.

For the immunoassay, 1.0 μL of the h-IgG solution of different concentrations was spotted on a dry nitrocellulose strip. The strip was incubated for 1 h in a blocking buffer solution containing 1% BSA, 0.5% Tween 80, and 10 mM Tris-HCl (pH 7.0). The strip was then incubated for 2 h with the Au-antibody solution that was diluted by 5−10 times using 0.5% Tween 80 solution. Next, the strip was washed with Tris buffer solution (pH 7.0) containing 0.5% Tween 80. The strip was then treated with a silver developer solution for 1−2 min and washed with deionized water 3−4 times. The silver developer solution was freshly prepared by mixing Tween 80, $AgNO_3$, and ascorbic acid to give final concentrations of 0.5%, 1 mM, and 1 mM, respectively.

Instrumentation. UV−vis absorption spectra were recorded using an Agilent 8453 spectrophotometer in a 1 cm quartz cell. A FEI Technai G2 transmission electron microscope was used for transmission electron microscopy (TEM) studies. Samples were prepared by placing a drop of the diluted particle solution on a carbon-coated copper grid. A concentrated solution (5−10 mg/mL) was used in the nuclear magnetic resonance (NMR) spectroscopy (Brucker AV-400 instrument (400 MHz)). DLS samples were first filtered through a Millipore syringe filter (0.2 μm pores) and then characterized with a Model BI-200SM instrument (Brookhaven Instrument Corporation). Solid powder samples were used for photoacoustic Fourier transform infrared (FTIR) spectroscopy (Digilab FTS 7000 Series spectrometer with a MTEC Model 300 photoacoustic cell) and X-ray diffraction (XRD) studies (Siemens D5005 diffractometer). Cell imaging was performed using an Olympus microscope IX71 with a DP70 digital camera.

Results

Silica Coating. The silica-coating method involves the condensation of alkoxysilanes on the nanoparticle surface. Various types of functional silanes were used, all of which have trimethoxysilyl or silanol groups at one end and an amino or phosphonate group at the other end. Trimethoxysilyl or silanol groups would undergo hydrolysis in a basic/acidic medium to form a silica shell. Two different strategies were used to initiate the silica polymerization on the nanoparticle surface. For oxide nanoparticles, silanization involved the condensation of silanes with the hydroxyl groups on the particle surface.[12] In the case of Au, Ag, and ZnS−CdSe, MPS was used as a linker silane.[10d,e,15a] The thiol group of this linker silane would be chemisorbed onto the non-oxide nanoparticle surface, and the trimethoxysilane groups would initiate the silica shell formation on the nanoparticle surface.

We have optimized the silanization conditions to obtain water-soluble nanoparticles. Two important steps were identified in the silane conjugation scheme. First, the starting nanoparticles had to be rid of excess ligands. As-synthesized particles of Fe_3O_4 and ZnS−CdSe have free ligands such as long-chain amine/acid, trioctylphosphine, and trioctylphosphine oxide.[3−5] Although these ligands were essential for the synthesis of high-quality near-monodispersed nanoparticles, their presence in excess would adversely impact the silica-coating process. In the control experiments of silanization of as-synthesized particles, insoluble particle aggregates were formed along with free silica. This finding indicated that the presence of free ligands disrupted the silane-coating process and induced silica nucleation beyond the nanoparticle surface. When silica coating was performed after the removal of free ligands (by successive washes as described in the Experimental Procedures), water-soluble particles were attained.

Second, we noted that silane hydrolysis could be controlled by varying the temperature, heating time, and base concentration. Alkylamine or aminosilane could act as an ideal base for the slow catalytic hydrolysis of alkoxysilane at 65−70 °C. Use of TMAH as a base or increasing the temperature beyond 80 °C increased the rate of silane hydrolysis, leading to uncontrolled hydrolysis and the formation of partially or completely insoluble particles. Under the optimal conditions described in the Experimental Procedures, the nanoparticle−silane conjugate began precipitating within 3−5 min of reaction, and the precipitation was completed within 15−30 min. This slower hydrolysis rate was ideal as the hydrolysis could be stopped at any time by quenching the reaction to room temperature or by separating the precipitate from the solution. Further heating of the precipitated nanoparticle−silane conjugates without separating them from free silanes could lead to intraparticle cross-linking via hydrolysis (step II in Figure 1b), without significant interparticle cross-linking. This was confirmed by the formation of more stable colloids, without particle−particle aggregation.

The successful coating of nanoparticles with a thin silica shell was confirmed by characterizing the particles after the coating process. TEM, XRD, and DLS were employed to characterize the particle size, crystallite size, and crystalline structure (Figure 2 and Supporting Information (SI) Figures S1−S4). NMR and FTIR spectra were used to elucidate the presence of the organic ligand shell (SI Figures S5 and S6). They showed that the original ligands used in particle synthesis were absent in the silanized particles and that only the silanes were present. Characteristic silica and silanol peaks were observed in the FTIR spectra of coated nanoparticles. No significant difference was observed in the NMR and FTIR spectra of the silica-coated nanoparticles derived with one- or two-step silanization.

The coating process was also optimized for long-term colloidal stability. Oxide particles subjected to one-step silanization showed a relatively low colloidal stability, precipitating from aqueous solution after several weeks. In contrast, those subjected to two-step silanizaton were stable as a colloidal solution for several months. The reverse trend was observed for Au, Ag, and ZnS−CdSe (i.e., one-step silanization produced completely water-soluble particles, whereas two-step silanization generated only partially water-soluble particles).

Milligram to multigram scale synthesis of functionalized nanoparticles has been attained by our silanization method. We have applied the same scheme with other functional silanes or silane mixtures (e.g., amine, phosphonate, glycidoxy, PEG, halide, gluconamide, pyridine, acryloyl, and long-chain hydrocarbon), and the respective functionalized nanoparticles have been successfully derived. The silanization scheme for Fe_3O_4 was also effectively applied to other hydrophobic oxides, such as MnO and ZnO, to obtain water-soluble nanoparticles. These results demonstrated the versatility of our silanization scheme.

The present scheme of the toluene-phase silica coating has several advantages and differences from the reverse micelle-based silica coating reported earlier.[13b,c,15h,l,m] Reverse micelle-based coating is a modification of Stöber's approach[17] and involves TEOS. This silane would be ideal for thick silica coating (2−50 nm); it gave rise to multicore particles with a poor colloidal stability when employed in attempts to derive a thin silica coating. This was because TEOS would tend to extend polymerization in three dimensions. Another limitation of the reverse micelle was its high sensitivity to reagents such as silanes and base catalysts. Thus, only limited experimental conditions, such as room temperature and dilute solutions of particles and silanes, could be used for silica

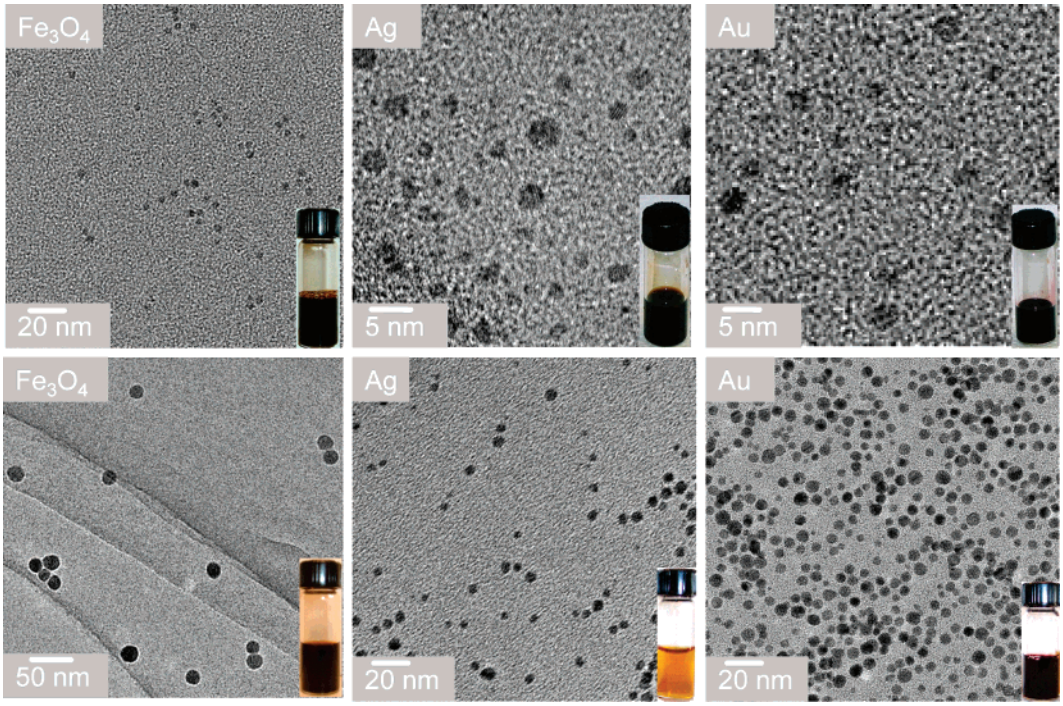

Figure 2. Representative TEM micrographs of various silanized nanoparticles. (Inset) Respective optically clear aqueous solutions containing 10−20 mg/mL of nanoparticles.

Table 1. TEM Crystallite Size and DLS Particle Size (nm) before and after Silica Coating[a]

	Au	Ag	Fe_3O_4	ZnS−CdSe
TEM crystallite size (DLS particle size) before coating	2 ± 1 (5 ± 2), 6 ± 1 (8 ± 2)	2 ± 1 (6 ± 2), 5 ± 2 (7 ± 2)	5 ± 0.5 (6 ± 3), 15 ± 1 (17 ± 2), 25 ± 2 (28 ± 4)	3 ± 1 (6 ± 2)
TEM crystallite size (DLS particle size) after coating	4 ± 2 (8 ± 2), 7 ± 1 (15 ± 2)	4 ± 2 (12 ± 4), 6 ± 2 (15 ± 4)	5 ± 0.5 (11 ± 3), 15 ± 1 (24 ± 4), 25 ± 2 (35 ± 5)	3 ± 1 (12 ± 3)

[a] 100−200 particles were counted in TEM micrographs to determine the average crystallite size. DLS particle sizes are noted in parentheses.

coating. Otherwise, particle precipitation or insoluble particle aggregates would develop. The toluene-phase silanization presented here could be performed with a much higher concentration (1−50 mM) of nanoparticles and silane reagents and allow for heating during silane hydrolysis. This provided silica-coated particles with a large-scale synthesis. Use of trimethoxysilanes and trihydroxysilanes would enable polymerization to be terminated at early stages for the formation of a thinner silica shell.

Size Characterization. Silanized particles were characterized by TEM and DLS for particle size and size distribution. The core size remained unchanged for QD and Fe_3O_4 but increased by 1−3 nm for Au and Ag due to the thermal effects in silanization (Table 1). Previous work has shown that the heating of thiol-functionalized polydispersed Au and Ag particles would lead to the formation of monodispersed particles due to Ostwald ripening.[4c,18] In our case, heating has two effects: enhanced silane hydrolysis and narrowing of the particles size distribution (for Au and Ag). TEM micrographs illustrated that the particles were isolated from each other (Figure 2). The silica shell was not notable even in high-resolution TEM, indicating that the shell was very thin and amorphous (see SI Figures S2 and S3). A similar observation was noted by others.[15b] Thus, the dimensions observed in TEM mainly corresponded to the core size, which were in agreement with the XRD grain size obtained from the peak broadening analysis (SI Figure S1). DLS of the concentrated dispersions showed that the particle size ranged from 5 to 30 nm, depending on the core size (see SI Figure S4). DLS results represented the overall particle size (i.e., including the silica shell), which was ∼4−10 nm greater than the TEM crystallite size (see Table 1). The overall particle size determined by DLS was ∼10−30 nm, which was smaller than that derived by the reverse micelle method due to the thinner silica shell achieved with our method.

Optical Properties. The concentrated solution of silanized Au was pink and that of Ag was dark brown or yellow depending on the core size. The solutions of silanized Fe_3O_4 with 5 and 12 nm cores were black and brown, respectively. Characteristic surface plasmon bands were noted in the UV−vis absorption spectra of silanized Au and Ag (Figure 3a,b). Similar bands were observed earlier for Au and Ag nanoparticles of various sizes;[4c] narrow bands indicate minimal particle aggregation. Silanized Fe_3O_4 showed absorbance without any characteristic peaks in the visible range. Silanized QDs have characteristic size-dependent optical

(18) (a) Zhong, C. J.; Zhang, W. X.; Leibowitz, F. L.; Eichelberger, H. H. *Chem. Commun.* **1999**, 1211. (b) Lin, X. M.; Sorensen, C. M.; Klabunde, K. J. *J. Nanopart. Res.* **2000**, *2*, 157. (c) Shimizu, T.; Teranishi, T.; Hasegawa, S.; Miyake, M. *J. Phys. Chem. B* **2003**, *107*, 2719.

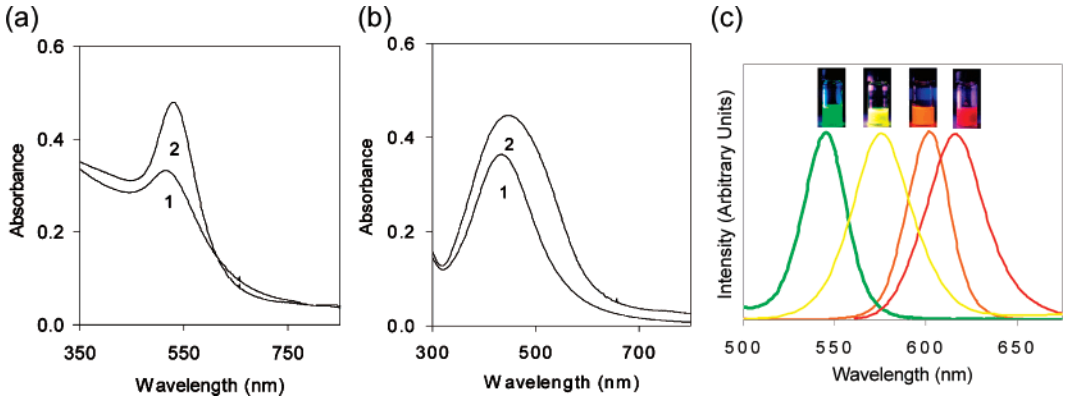

Figure 3. UV−vis absorption spectra of (a) silica-coated Au and (b) silica-coated Ag with (1) 5 nm and (2) 8 nm cores. (c) Emission spectra of silica-coated ZnS−CdSe nanoparticles of different sizes. (Inset) Respective MES buffer solutions under UV excitation.

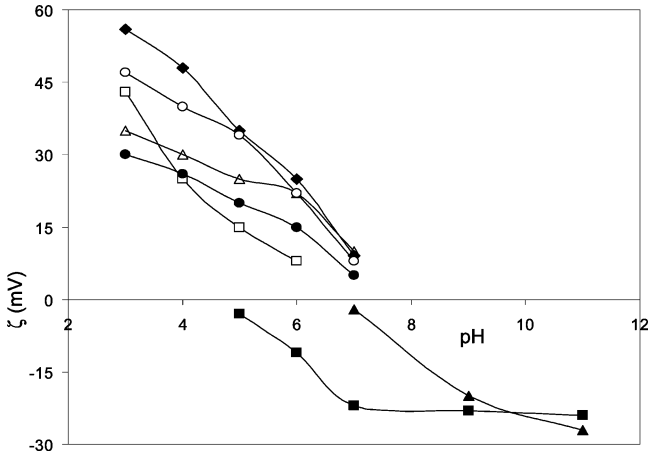

Figure 4. pH-Dependent surface charge of silica-coated nanoparticles of (▲) PO_3-functionalized Fe_3O_4, (△) NH_2-functionalized Fe_3O_4, (■) PEG-PO_3-functionalized Fe_3O_4, (□) PEG-NH_2-functionalized Fe_3O_4, (♦) PEG-NH_2-functionalized QD, (○) NH_2-functionalized Ag, and (●) NH_2-functionalized Au.

properties, emitting green, yellow, orange, or red depending on the core size (Figure 3c). The quantum yield was determined to be 15−30% depending on the core size; fluorescein was used as the standard.

Surface Charge and Colloidal Stability. The silanized particles have a positive or negative surface charge (varying from +55 to −30 mV), depending on the solution pH and type of silane used (Figure 4). Amino silane produced primary amine-functionalized particles, which were protonated in acidic pH to give positively charged particles. As the solution pH gradually increased, the primary amines were deprotonated, leading to a gradual decrease in the surface positive charge. The NH_2-functionalized particles have a lower colloidal stability and slowly precipitated from solution at a pH of 6−7, as their surface charge approached zero.

Phosphonate silane produced negatively charged particles due to the deprotonation of the phosphonate group. The PO_3-functionalized particles were stable in the pH range of 7−11. In acidic pH, the phosphonate groups became protonated, and the surface charge was reduced, causing the particles to precipitate slowly from solution. Introducing the PEG functional group along with primary amine or phosphonate silane enhanced the colloidal stability substantially in the pH range of 5−8.

The colloidal stability of silanized particles was studied in various buffers (such as borate, Tris, HEPES, MES, and phosphate), at different pH values, and at a high NaCl concentration. Primary amine-functionalized Au, Ag, and Fe_3O_4 were stable in all the acidic buffers (except phosphate buffer) for more than a year in the presence of a high salt concentration (1 M NaCl) and in acidic pH without any trace of precipitation. However, these particles would precipitate immediately if the solution pH was increased to 7 or above. PEG-NH_2-functionalized Au, Ag, and Fe_3O_4 were stable in neutral pH buffers. While NH_2-functionalized particles were unstable in phosphate buffer, the PO_3-functionalized Fe_3O_4 particles were very stable in phosphate buffer. The colloidal stability of silanized QDs was relatively poor as compared to the other nanoparticles. Silanized QDs were stable in acidic buffer (HEPES and MES) for several months but experienced fluorescence quenching over time. PEG-NH_2-functionalized QDs have a better solubility in borate and Tris buffers (pH 7.0), but they also precipitated after several weeks.

Conjugation Chemistry and Biolabeling Applications. To demonstrate that the silanized nanoparticles could be further functionalized with various biomolecules of interest, conventional bioconjugation schemes were employed successfully to derive biotinylated and antibody-conjugated Au, Ag, Fe_3O_4, and QDs. Two NHS based reagents, NHS-PEG-biotin and NHS-PEG-NHS, were used. NHS reacted with the primary amine on the nanoparticle surface, creating a covalent linkage via amide bond formation. Similarly, bifunctional PEG would create a linkage between nanoparticle and antibody. PEG functional groups increased the colloidal stability of nanobioconjugates. The colloidal stability of silanized nanoparticles was retained during the conjugation and other processing steps, such as dialysis and Sephadex column separation. The conjugated biomolecules also retained their biochemical activity (Figure 5). Anti-h-IgG-functionalized Au nanoparticles were used successfully for the detection of h-IgG (Figure 5c).

Discussion

Coating Chemistry. Syntheses of metallic, oxide, and semiconducting nanoparticles in the organic phase offered several advantages. They provided crystalline, near-monodispersed particles with a tunable size in the range of 1−20 nm in a milligram to gram scale.[3−5] The resulting nanoparticles were hydrophobic in nature due to the surfactant coating. They were soluble in organic solvents (such as

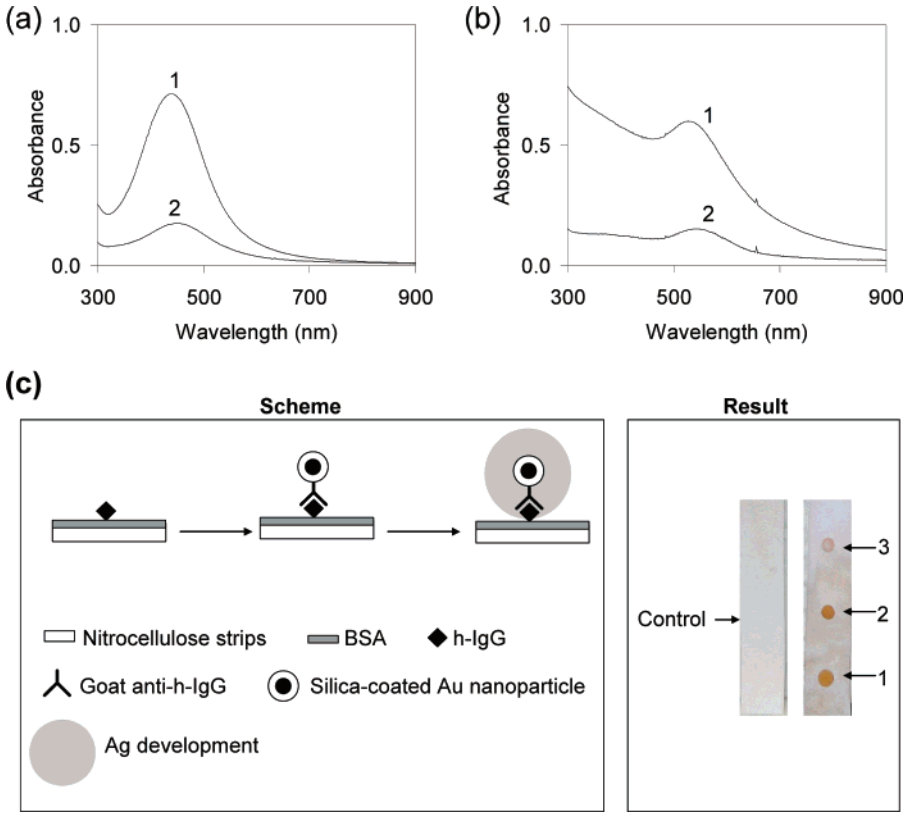

Figure 5. Biotinylated (a) Ag and (b) Au nanoparticles (1) in aqueous borate buffer and (2) in the presence of avidin. (c) Detection of (1) 100 ng/mL, (2) 10 ng/mL, and (3) 1 ng/mL of protein with antibody-functionalized Au nanoparticles.

hexane, toluene, and chloroform) but insoluble in alcohol and water. In this work, we have selected toluene as the solvent for silica coating since both nanoparticles and most silanes are highly soluble in toluene. We also found that the silanized nanoparticles would precipitate from toluene, thus separating them from the unreacted silanes. This separation scheme provided two advantages. First, it minimized the particle−particle aggregation during the coating processes as the precipitate could be easily separated from the silane precursors. Most of the previous research utilized polar solvents as the medium for silica coating, wherein particle−silica conjugates were difficult to be separated from free silanes at the intermediate stage, thus leading to either thick silica coating or insoluble products due to particle−particle cross-linking. Second, our approach simplified the silica-coating scheme, allowing silanization of Au, Ag, and QD to be achieved in one-pot or -step processes. We could use large excesses of silane precursors without worrying about increasing the silica shell thickness. Continued reaction of the precipitated particles in the presence of excess silane in toluene also did not significantly increase the particle−particle cross-linking but promoted the polycondensation of the silica shell surrounding the particles.

To achieve good colloidal stability, Au, Ag, and QDs just needed step I of the silanization scheme, while oxide nanoparticles required two-step silanization. This was because the silanization of Au, Ag, and QDs involved both MPS and AEAPS, where the mercapto group of MPS would adsorb onto the nanoparticle surface, while the trimethoxy silyl group from each silane would condense around the particle surface. The relatively lower colloidal stability of QDs could be attributed to the less effective chemisorption of thiols on the ZnS−CdSe surface. In the case of oxide nanoparticles, only one silane was involved, which was not effective enough for capping the particle surface in one step, thus requiring step II for intraparticle cross-linking.

Silanization of particles <10 nm was found to be most successful, whereas silanization of particles >15 nm often led to insoluble precipitates. This might be due to the lower colloidal stability of larger nanoparticles in toluene, particularly during the ligand-exchange step with silane. Thus, these larger particles would precipitate before silica coating began, and most of the silica was formed as a separate phase from the particles. The larger silanized particles also have a higher surface charge (>50 mV in aqueous phase), which might have made them unstable during silanization in toluene.

Properties of Functionalized Nanoparticles. Silanized nanoparticles were unique and different from conventional colloids in many ways. They were 10−30 nm in size, smaller than the conventional silica-coated nanoparticles. They have excellent water solubility and long-term colloidal stability. We noticed that the colloidal stability of particles with a surface charge greater than ±40 mV was very sensitive to the salt or buffer present and to the pH value. Larger particles with cores of >10 nm tended to have such high surface charges and thus possessed a lower colloidal stability and water solubility. In contrast, smaller particles 10−20 nm in size have a more desirable surface charge of ±10−30 mV, which provided a greater colloidal stability and water solubility. The surface charge of the particles could be tuned from positive to negative by changing the surface functional groups and/or solution pH. The silanized nanoparticles could

be precipitated and redispersed many times by simply varying the solution pH or ionic strength. The water solubility of amine-, PEG-, and phosphonate-functionalized nanoparticles was ~10−100 mg/mL, depending on the particle size, pH, and ionic strength. The amine-phosphonate, amine-dimethylamine, and amine-PEG-bifunctionalized nanoparticles were water-soluble and stable over a wide range of pH values, from acidic to basic media. This would be very useful for bioconjugation as the bioconjugated particles would maintain their solubility in water.

We have quantified amine functionality by fluorescamine titration. This was performed for a ZnO system (data not shown here) as the fluorescence quenching of the fluorescamine−amine complex was noted for other systems. Various ratios of amino and phosphonate silanes were used during silanization, and the average number of amine groups per particle could be varied between 10 and 1000, which would be useful for tailoring the number of biomolecules on the particle surface.

Soluble and functionalized nanoparticles were conjugated to biotin and anti-h-IgG, and the bioconjugated nanoparticles were water-soluble in spite of the presence of a water-insoluble biofunctionality (e.g., biotin). This was due to the presence of additional water-soluble functional groups (e.g., phosphonate, ammonium, and PEG) on the nanoparticle surface and the relatively low number of biomolecules per particle (as compared to water-soluble functional groups). This result was significant as compared to many previous reports, whereby a high number of biomolecules per particle has led to reduced particle solubility.[7b]

As designed, our biotinylated Ag and Au nanoparticles precipitated in the presence of avidin. On the basis of specific biotin−avidin interactions, these biofunctionalized systems would indicate a reduced absorbance upon the detection of avidin (Figure 5a,b). The anti-h-IgG-functionalized Au nanoparticles also demonstrated the effective labeling of h-IgG. Silanized Au could act as a seed for the particle enlargement step during the silver enhancement, without any inhibiting effect from the silica shell (Figure 5c). The antibody-functionalized Au nanoparticles successfully detected proteins at a concentration as low as 1 ng/mL. These studies illustrated that our silanized nanoparticles could be developed as functional nanoparticles for various biolabeling applications.

Conclusion

In this study, we have demonstrated a generalized silanization method, which could be broadly applied to different silanes to functionalize a wide variety of hydrophobic nanoparticles. This new approach eliminated any water-insoluble nanoparticle byproducts. The silanized nanoparticles were highly soluble and stable under a broad range of experimental conditions. The number of surface functional groups per particle could be controlled to attach biomolecules of a desired quantity. A variety of biochemicals could be binded covalently to the surface of the functionalized nanoparticles for biolabeling and biosensing applications.

Acknowledgment. The authors thank Drs. S. Tamil Selvan, Yuangang Zheng, and Hsiao-hua Yu for helpful discussions and Dr. Yu Han for TEM characterization. This work was supported by the Institute of Bioengineering and Nanotechnology (Biomedical Research Council, Agency for Science, Technology and Research, Singapore).

Supporting Information Available: TEM of Fe_3O_4 nanoparticles of various sizes before and after silica coating; XRD, high-resolution TEM, DLS, NMR, and photoacoustic FTIR data of silica-coated nanoparticles. This material is available free of charge via the Internet at http://pubs.acs.org.

CM071368Z